SEE COMMENTARY

Neurovascular coupling to D2/D3 dopamine receptor occupancy using simultaneous PET/functional MRI

Christin Y. Sander[a,b,1], Jacob M. Hooker[a], Ciprian Catana[a], Marc D. Normandin[c], Nathaniel M. Alpert[c], Gitte M. Knudsen[d], Wim Vanduffel[a,e], Bruce R. Rosen[a,f], and Joseph B. Mandeville[a]

[a]Athinoula A. Martinos Center for Biomedical Imaging, Department of Radiology, Massachusetts General Hospital, Charlestown, MA 02129; [b]Department of Electrical Engineering and Computer Science, Massachusetts Institute of Technology, Cambridge, MA 02139; [c]Division of Nuclear Medicine and Molecular Imaging, Massachusetts General Hospital, Boston, MA 02114; [d]Neurobiology Research Unit and Cimbi, Rigshospitalet, University of Copenhagen, DK-2100 Copenhagen, Denmark; [e]Laboratory of Neuro- and Psychophysiology, Medical School, Katholieke Universiteit Leuven, 3000 Leuven, Belgium; and [f]Division of Health Sciences and Technology, Harvard-Massachusetts Institute of Technology, Cambridge, MA 02139

Edited[†] by Joanna S. Fowler, Brookhaven National Laboratory, Upton, NY, and approved April 30, 2013 (received for review December 17, 2012)

This study employed simultaneous neuroimaging with positron emission tomography (PET) and functional magnetic resonance imaging (fMRI) to demonstrate the relationship between changes in receptor occupancy measured by PET and changes in brain activity inferred by fMRI. By administering the D2/D3 dopamine receptor antagonist [^{11}C]raclopride at varying specific activities to anesthetized nonhuman primates, we mapped associations between changes in receptor occupancy and hemodynamics [cerebral blood volume (CBV)] in the domains of space, time, and dose. Mass doses of raclopride above tracer levels caused increases in CBV and reductions in binding potential that were localized to the dopamine-rich striatum. Moreover, similar temporal profiles were observed for specific binding estimates and changes in CBV. Injection of graded raclopride mass doses revealed a monotonic coupling between neurovascular responses and receptor occupancies. The distinct CBV magnitudes between putamen and caudate at matched occupancies approximately matched literature differences in basal dopamine levels, suggesting that the relative fMRI measurements reflect basal D2/D3 dopamine receptor occupancy. These results can provide a basis for models that relate dopaminergic occupancies to hemodynamic changes in the basal ganglia. Overall, these data demonstrate the utility of simultaneous PET/fMRI for investigations of neurovascular coupling that correlate neurochemistry with hemodynamic changes in vivo for any receptor system with an available PET tracer.

dynamic binding potential | displacement | monkey | NHP

The neural basis of functional magnetic resonance imaging (fMRI) signals has been a topic of extensive investigation. Experimental correlations of fMRI signals or cerebral blood flow with relative changes in glucose or oxygen utilization (1–3) have been performed to determine whether hemodynamic responses reflect a coupling with metabolism—a hypothesis with a long history (4). To relate hemodynamic responses more directly to neural circuitry, fMRI or optical imaging signals have been correlated with electrophysiology, using graded levels of stimulation in preclinical models (5–7). These results generally demonstrate a monotonic coupling between electrical activity and evoked cortical hemodynamic responses, using sensory stimuli. However, the methodology is not readily extensible to human subjects, and the implications of such studies are difficult to generalize to pharmacotherapies or other drug stimuli that target specific neurotransmitter systems.

Recent technological advances in multimodal imaging have enabled the simultaneous acquisition of MRI and positron emission tomography (PET) data (8). One of the motivations for conjoining these modalities was the potential for new insights into neural function based upon the complementary natures of PET and fMRI. In activation paradigms, fMRI provides excellent spatio-temporal resolution for localizing changes in brain activity but offers little insight into the underlying neurotransmission. Conversely, although PET has more limited temporal and spatial resolution for functional measurements, it offers high sensitivity and neurochemical specificity. Together, PET and MRI measures have the potential to help clarify the neurochemical basis of changes in fMRI signal induced by selective exogenous ligands or endogenous neurotransmitter. Perhaps because combined PET/MRI systems have become available only recently, there have been no reports to date that have dynamically compared the functional output reported by fMRI with in vivo occupancy for any neuroreceptor system targeted by a selective ligand.

The dopamine (DA) system has been a primary target of PET studies due to its role in numerous diseases, including Parkinson disease, schizophrenia, and behaviors related to natural rewards and drug abuse. The basal ganglia present an ideal target system for initial PET/fMRI studies of neurovascular coupling, because this system has been studied widely in humans and nonhuman primates (NHPs), using PET radiotracers that have been thoroughly characterized (9). fMRI signals strongly correlate with evoked DA in rodents under some circumstances (10), suggesting that DA is driving the fMRI response. Stimulation of D2/D3 dopamine receptors (D2/D3R) produces inhibition of basal ganglia in fMRI studies in rodents (11, 12). This finding is consistent with G-protein–coupled pathways leading to D2/D3R-mediated inhibition of adenylate cyclase and cyclic AMP, a second messenger in the ATP pathway leading to energy production (13).

In this study, responses of the dopaminergic system in NHPs were assessed with PET/fMRI to characterize the dynamic relationship between hemodynamic responses and changes in neurochemistry. The PET ligand [^{11}C]raclopride (RAC), a selective D2/D3R antagonist, was administered at decreasing specific activities (i.e., increasing total mass doses) to evoke fMRI responses. The latter were compared to receptor occupancy measures from PET in the domains of time, space, and dose. Thereby, we test the hypothesis that fMRI signal changes are correlated with DA displacement in each of these domains. This study initiates a new methodology for investigating neurovascular/neurochemical coupling in health and disease, using simultaneous PET/fMRI.

Results

Fig. 1 demonstrates the basic paradigm and hypothesis employed in this study. With a very low mass of [^{11}C]RAC, the PET signal is sensitive to available D2/D3R in the baseline state (Fig. 1*A*). Due to much higher density of D2R relative to D3R in caudate and putamen (14), [^{11}C]RAC-specific binding is highly weighted by D2R density in these regions. We hypothesize that increasing

Author contributions: C.Y.S., J.M.H., W.V., B.R.R., and J.B.M. designed research; C.Y.S., J.M.H., C.C., M.D.N., and J.B.M. performed research; C.C. and J.B.M. contributed new reagents/analytic tools; C.Y.S. and J.B.M. analyzed data; and C.Y.S., J.M.H., C.C., M.D.N., N.M.A., G.M.K., B.R.R., and J.B.M. wrote the paper.

The authors declare no conflict of interest.

[†]This Direct Submission article had a prearranged editor.

See Commentary on page 10888.

[1]To whom correspondence should be addressed. E-mail: csander@mit.edu.

This article contains supporting information online at www.pnas.org/lookup/suppl/doi:10.1073/pnas.1220512110/-/DCSupplemental.

NEUROSCIENCE

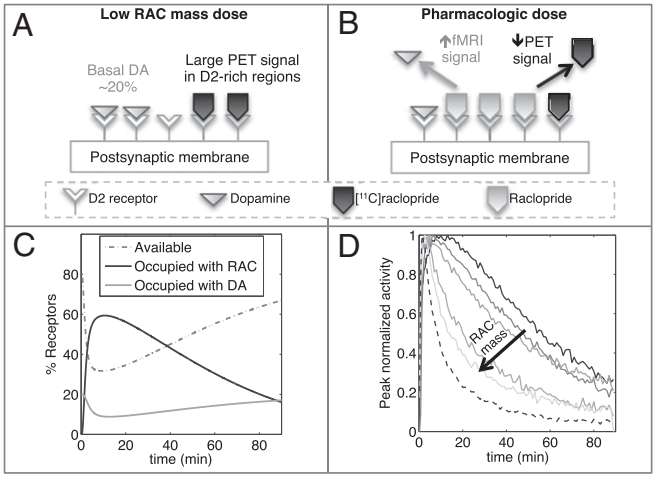


Fig. 1. Schematic illustrating the basic PET/fMRI paradigm. (*A*) [^{11}C]RAC binds specifically to available D2/D3R in the baseline state. (*B*) Antagonism at D2/D3R causes a positive fMRI signal, whereas unlabeled RAC competes with [^{11}C]RAC, decreasing the PET signal. (*C*) Simulations show the dynamics of RAC and DA occupancy at D2/D3R, together with available D2/D3R, all expressed as a percentage of total D2/D3R. (*D*) Experimental results show changes in the shape of PET TACs for whole putamen, normalized to peak, in order of increasing RAC mass dose (solid line to lines with light shading) and a low-mass cerebellum TAC (dashed line).

masses of nonradioactive RAC (decreasing specific activities) displace progressively more DA, reducing PET binding at D2/D3R, while invoking an fMRI signal (Fig. 1*B*). This is illustrated in the temporal domain by simulations of a two-tissue compartmental model (Fig 1*C*): The wash in/wash out of RAC causes a time-dependent displacement of basal DA from D2/D3R and a reduction of available D2/D3R. However, pharmacokinetics largely dictate the shape of time-dependent changes in specific binding, which differs only subtly vs. mass until high occupancies in simulations (Fig. S1 and Table S1).

Experimental PET time-activity curves (TACs) from five injections of [^{11}C]RAC with different specific activities in one NHP [male rhesus macaque 1 (M1)] are shown in Fig. 1*D* for whole putamen and normalized to peak activity, together with the low-mass cerebellum TAC as a reference. As the total injected mass of RAC increases, unlabeled RAC occupies progressively more binding sites and thus reduces specific binding by labeled RAC, so that putamen TACs start to resemble the shape of the nonspecific (cerebellum) TAC.

Kinetic Modeling Results. We hypothesized that changes in RAC-specific binding are related to fMRI responses under the assumption that DA displacement drives the fMRI signal. Hence, we employed two analyses within the simplified reference tissue model (SRTM) framework (15): (*i*) a conventional steady-state binding potential [binding potential (nondisplaceable) (BP_{ND})] analysis and (*ii*) an analysis based upon "dynamic binding potentials", $DBP_{ND}(t)$, as defined in Eq. **3** in *Materials and Methods*, to compare peak changes in PET binding with peak changes in fMRI signal.

Kinetic model fits are illustrated in Fig. 2 for three different RAC mass doses in M1. Dynamic analyses (Fig. 2 *B* and *C*) reduced the chi-square per degree of freedom (χ^2/DOF) and Akaike information criterion measures for all fits. Representative curve fits comparing the SRTM and dynamic analysis are shown in Fig. S2. Moreover, dynamic analyses of forward-model simulations determined that DBP_{ND}^{peak} consistently produced good agreement with true peak occupancies (Fig. S3), whereas analyses based upon BP_{ND} did not consistently reflect peak or average occupancies across all mass doses. For the low-mass RAC dose, DBP_{ND}^{peak} values from both animals averaged 4.2 ± 1.3 in putamen and 3.8 ± 1.3 in caudate, while BP_{ND} values averaged 4.3 ± 1.8 in putamen and 4.1 ± 1.9 in caudate. Average R_1 and k_2' parameters from the DBP_{ND} analysis were 0.93 ± 0.08 and 0.27 ± 0.30, respectively.

Temporal Correlation. Temporal responses from fMRI for whole putamen are shown in Fig. 3 *A* and *B* for the two highest-injected masses of RAC in one animal and are overlaid with approximations of specific binding ($\hat{S} = C_T - R_1 C_{REF}$), derived directly from PET TACs. Using this specific binding estimate allowed a direct temporal comparison of responses derived from PET and fMRI data. $\hat{S}$ provides a reasonably accurate index of specific binding as modeled with a two-tissue compartmental model (Fig. S4). The time courses of PET-specific binding estimates and fMRI responses resembled each other, as time-to-peak measures and durations were similar.

Fits to the fMRI temporal response and $DBP_{ND}(t)$ were determined by varying the time-to-peak (τ) of gamma-variate regressors ($t/\tau \cdot e^{-t/\tau}$) to optimize the goodness of fit to the data within the general linear model (GLM). For both fMRI and PET data, χ^2/DOF values were slowly varying functions of the time to peak. All χ^2/DOF values increased by less than 10% across a 4-min window centered upon the optimal value. Optimal time-to-peak values from fMRI and PET analyses differed by less than 4 min for each animal at the two highest doses, for which the fMRI signal was robust.

Spatial Correlation. Fig. 4, *Upper* shows parametric DBP_{ND}^{peak} maps from PET for four mass doses, and Fig. 4, *Lower* shows the corresponding fMRI maps in units of percentage of cerebral blood volume (%CBV). A *P*-value threshold of $P<0.03$, computed with a mixed-effects model (16) across two animals, was applied to all CBV maps. For the lowest RAC mass, the DBP_{ND}^{peak} maps exhibited high specific binding and a high binding potential in the striatum, but hardly any detectable fMRI signal. In the voxelwise maps, 49% of voxels within the putamen were above a value of DBP_{ND}^{peak} and 23% within the putamen exceeded a value of DBP_{ND}^{peak}. Results were reversed for the highest RAC mass dose, for which binding potential was very small, whereas fMRI reported a large positive change in CBV. The peak CBV response relative to baseline CBV averaged 9.8% ± 3.5% across whole putamen and 4.3% ± 1.7% across caudate. Voxelwise analysis showed that 45% of voxels within the putamen show CBV>8% and 19% of voxels in putamen recorded CBV>12%.

The high-binding regions of the striatum and the neurovascular responses were remarkably similar on the voxel-wise maps (Fig. 4). As mass dose increased, the specific binding signal in the striatum decreased visibly in the parametric DBP_{ND}^{peak} images, whereas CBV increased from no detectable signal to a prominent signal within the striatum.

Occupancies and Relationship to fMRI. Table 1 lists values for BP_{ND}, DBP_{ND}^{peak}, steady-state RAC occupancies $\hat{\theta}_{RAC}$, and peak occupancies $\hat{\theta}_{RAC}^{peak}$ (Eq. **4**) for whole putamen from the SRTM and the dynamic binding analysis, together with peak changes in

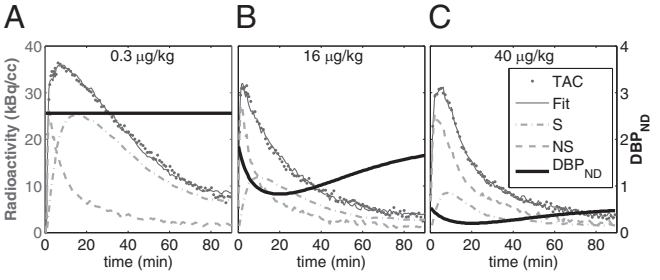


Fig. 2. (*A–C*) PET TAC for whole putamen in M1 (dots) for the lowest-mass dose (*A*) and the two highest masses (*B* and *C*) with fit to the data (solid lines). DBP_{ND}s (Eq. **3**) (shaded lines), together with SRTM estimates of nonspecific ($NS = R_1 C_{REF}$) or specific binding ($\hat{S} = C_T - R_1 C_{REF}$) are displayed over time. Dynamic binding analyses demonstrated an improved fit to data.

CBV for each RAC mass dose for both animals. BP_{ND}s extrapolated to true zero occupancy for whole putamen were 3.3 and 5.0 for NHPs M1 and M2, respectively. These were computed from five (M1) or four (M2) RAC mass doses with the Hanes–Woolf plot, in which $1/BP_{ND}$ is plotted vs. free ligand concentration in tissue. The latter was estimated from specific activity values and the first 60 min of data from the cerebellum TAC. On the basis of these extrapolated baseline binding potentials, occupancies for whole putamen ranged from ~7% to 91% for M1 and from <1% to 82% for M2. The average RAC dissociation constant K_D across animals was 1.9 ± 0.6 nM [assuming a RAC free fraction, $f_{ND} = 0.12$ (17)], which is within the range of literature values (18).

Fig. 5 *A* and *B* shows the relationship between peak RAC occupancies and peak %CBV changes for whole putamen and caudate in each animal. Data points were described by regression with a power law with two parameters: $(a \cdot (\hat{\theta}^{peak}_{RAC})^b)$. For M1, the exponent b was 1.7 and 1.4 in putamen and caudate, respectively, with R^2 values of 0.97 and 0.39. For M2, the corresponding exponents were 1.4 and 1.6, with R^2 values of 0.99 and 0.88. The regression with a power fit is concordant with a model describing the relationship between DA and RAC occupancy (Eqs. **S1** and **S2**). If we assume a twofold increase in extracellular DA due to RAC injection, model calculations and a corresponding power law fit predict an exponent of $b = 1.6$ (Fig. S5), which agrees with our experimental data.

From a regional analysis, we found that CBV^{peak} responses from the putamen region of interest (ROI) were much larger compared to caudate in both animals (Fig. 5). The putamen/caudate ratio of the CBV^{peak} response at 80% occupancy, estimated from the experimental data fit, was 2.2 ± 0.2. Including the fitted CBV^{peak} values for all occupancies between 50% and 100%, the average putamen/caudate ratio was 2.2 ± 1.7. Regional differences in receptor densities were 9% ± 2% less in caudate, as determined by baseline BP_{ND} values. These density differences alone do not provide an explanation for the much smaller functional response in caudate.

We conclude that there is a monotonically increasing relationship between RAC occupancy and changes in %CBV that showed a good fit to a superlinear function. Moreover, the magnitude of the CBV response for all RAC masses exhibited a regional dependence within the striatum.

Discussion

In this study, we investigated the relationship between neurovascular responses and receptor occupancies, using simultaneous PET/fMRI and variable mass doses of the D2/D3R antagonist RAC. As injected RAC mass dose was increased, the reduction in [^{11}C]RAC-specific binding correlated with CBV increases in the striatum spatially and temporally and with RAC mass dose. These data suggest that vascular responses to D2R-like antagonists are coupled to changes in neuroreceptor occupancy.

By directly comparing changes in neuroreceptor occupancy with a simultaneously induced functional response, we demonstrated an approach that can be employed widely using both antagonists and agonists. This opens up the possibility of probing mechanisms of neurovascular coupling or investigating brain circuitry by relating selective neuroreceptor binding to local and distant functional responses. Studies of this design can be used to develop multireceptor models that describe the fMRI response to endogenous neurotransmitter (19) to clarify the neurochemical basis of behaviors like reward (20, 21). Finally, simultaneous PET/fMRI studies using targeted PET ligands may provide information about basal receptor occupancy, a quantity that is not routinely measured by PET alone.

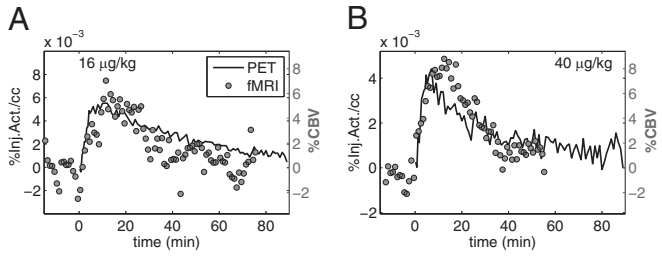


Fig. 3. (*A* and *B*) Temporal responses from PET-specific binding estimate ($\hat{S} = C_T - R_1 C_{REF}$, solid line), derived from experimental TACs, overlaid with CBV changes (1-min bins, shaded circles) for putamen for two high RAC masses. Time courses from CBV and $\hat{S}$ resemble each other.

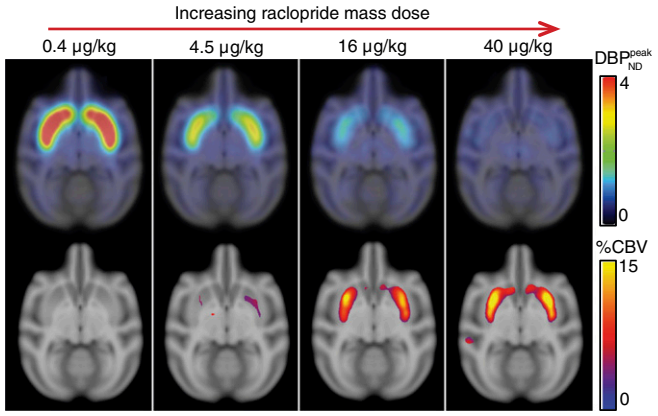


Fig. 4. (*Upper*) DBP^{peak}_{ND} parameter maps from PET data, overlaid on an anatomical MR atlas. (*Lower*) Maps of $\%CBV^{peak}$ change from fMRI data, windowed by a *P*-value map with $P<0.03$. All maps are created from data from two animals with a mixed-effects model. Similarities in the spatial distribution of PET/fMRI signals and the dose dependencies support the idea that antagonism of RAC at D2/D3R is elicited by the CBV changes.

Regional Dose Response. The maps of DBP_{ND} and %CBV in Fig. 4 each showed localized signals in striatal regions that exhibited a strong dependence on injected RAC mass. At low injected masses, DBP_{ND} maps showed high specific binding indicative of a large number of available receptors in basal ganglia, as expected. At high RAC masses, specific binding of [^{11}C]RAC was decreased by competition with unlabeled RAC. However, fMRI showed progressively larger increases in CBV at higher-mass doses that presumably reflect transient decreases of DA basal occupancy at D2/D3R. Because DA produces an inhibitory effect at D2/D3R, an explanation for the increase in CBV is that RAC blocks the inhibitory effect of DA upon D2/D3R. Thus, fMRI responses were observed predominantly in regions with high D2/D3R density.

Temporal Comparisons. The temporal response of the fMRI signal closely matched the kinetics of [^{11}C]RAC-specific binding estimates (Fig. 3). The temporal correlation is intriguing given the numerous physiological mechanisms that could cause temporal responses from the two modalities to diverge. For instance, a large dose of an agonist might promote receptor internalization. This mechanism has been suggested to explain the prolonged decrease in raclopride displacement following infusion of a large dose of amphetamine (22). With internalization, fMRI signal should be shortened in time, so that divergent temporal responses could offer insight into dynamic physiological adaptations like agonist-induced receptor internalization. However, our data show that a D2/D3 antagonist produces changes in binding potentials and fMRI signals that are well matched in time, which is consistent with a classical competition model (22) between RAC and DA for synaptic binding sites.

Neurovascular Coupling Mediated by D2/D3R Antagonism. In this study, data showed a monotonically increasing relationship between changes in CBV and RAC occupancies in subregions of basal ganglia. A postulate of linearity between tissue function and receptor occupancy was proposed as early as 1937 (23). For

Table 1. Summary of parameters and outcomes of the PET/fMRI paradigm for putamen in two animals (M1 and M2)

Study parameters and outcomes	Dose 1		Dose 2		Dose 3		Dose 4	
Study parameters*								
Injected RAC mass, μg/kg	0.3	0.3	4.5	4.5	16	16	40	40
Specific activity, μCi/nmol	1,350	1,350	53	53	8.9	8.9	6	6
Study outcomes	M1	M2	M1	M2	M1	M2	M1	M2
BP_{ND}	3.0	5.6	1.8	3.2	1.1	1.6	0.3	0.9
DBP_{ND}^{peak}	3.3	5.1	1.6	2.4	0.8	1.1	0.2	0.6
RAC occupancies† $\hat{\theta}_{RAC}$, %	0	0	40	43	63	71	90	84
Peak RAC occupancies† $\hat{\theta}_{RAC}^{peak}$, %	0	0	50	52	74	77	94	88
Peak ΔCBV, %	0.5‡ ± 0.3	−1.1‡ ± 0.4	2.2	5.8	5.6	10	7.3	12

*Average values from studies in two animals.
†Occupancies are computed relative to dose 1.
‡Average CBV from repeated studies.

pharmacological stimuli, receptor occupancy is an important synaptic quantity that underlies the genesis of a functional response. Moreover, correlations between hemodynamics and electrophysiology have shown that vascular responses are monotonically related to integrative synaptic quantities like local field potentials and multiunit activity (5–7, 24).

As a basis for discussion of the observed CBV-occupancy relationship, we propose a model for the fMRI response: CBV changes (ΔCBV) are driven by relative changes in receptor occupancies ($\Delta\theta$) and are scaled by ligand efficacies (ε), the local density of receptors (B_{max}), and excitatory/inhibitory neurovascular coupling constants (N). In a general framework, CBV changes due to exogenous or endogenous agonists reflect the sum of influences mediated by multiple receptor subtypes:

$$\Delta\mathrm{CBV} = \sum_{\mathrm{i=receptors}} \sum_{\mathrm{j=ligands}} N_i \varepsilon_{i,j} B_{max,i} \Delta\theta_{i,j}. \quad [1]$$

Antagonists like RAC have affinity but no efficacy at target receptors. However, RAC produces a physiological response by displacing DA. As a first step, we adopt a first-order (linear) approximation for our results that ignores any additional DA release ($\Delta\theta_{DA} = -\theta_{RAC}\theta_{DA}^{(0)}$; Eq. **S3** and Fig. S5) and Eq. **1** simplifies to

$$\Delta\mathrm{CBV} = -N_2 B_{max,2} \theta_{DA}^{(0)} \theta_{RAC}. \quad [2]$$

This description relates a positive ΔCBV to RAC occupancy, basal DA occupancy, and B_{max} via an inhibitory N_2.

The precise nature of the relationship between θ_{RAC} and the change in DA occupancy should be dependent on the magnitude of additional DA release induced by the binding of RAC to presynaptic autoreceptors (25). A classical competition model predicts that changes in fMRI signal are insensitive to DA release at very high RAC occupancies. At moderate occupancies, increased synaptic DA will more effectively compete with RAC, causing the relationship between DA and RAC occupancies to become superlinear (Fig. S5). This effect may explain the superlinear correlation between RAC occupancy and CBV in Fig. 5.

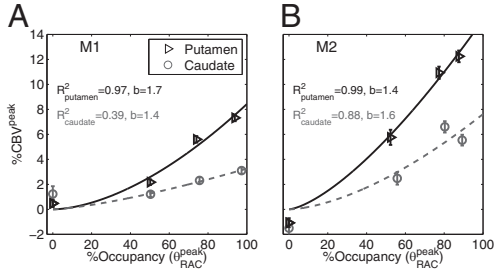


Fig. 5. (*A* and *B*) %CBV^{peak} vs. occupancy can be approximated by a power-law fit (with exponent b) for putamen and caudate ROIs for M1 and M2. Data show a monotonically increasing relationship, with putamen exhibiting approximately twice the CBV magnitude compared to caudate. Error bars show within-session uncertainty from the GLM analysis and SEM for repeated fMRI studies with the lowest RAC mass dose.

Basal Dopamine Occupancy. As observed from the CBV-occupancy plot (Fig. 5), caudate exhibited a remarkably smaller CBV increase than putamen with pharmacologic doses of RAC. The proposed coupling model from the previous section provides a potential explanation for this difference by showing that both receptor density and basal D2/D3R occupancy affect the CBV response. We can apply Eq. **2** to calculate the ratio of basal D2/D3R occupancy between putamen and caudate on the basis of our study data: Taking into account a small difference in receptor densities from our PET measurements (9% fewer receptors in caudate), this ratio is 2.0. Several studies have measured higher levels of basal DA in putamen compared to caudate, using microdialysis in NHPs in vivo (26, 27), with basal DA levels up to 2-fold higher in the putamen. Further evidence of higher basal D2/D3R occupancy in putamen is provided by human postmortem (28) and PET studies with basal DA depletion (29); both methods showed a 1.3- to 1.5-fold difference. Conversely, some studies indicate similar levels of basal DA or basal D2/D3R occupancy in putamen/caudate (30–32). Our results suggest that PET/fMRI measurements of this type offer the potential to noninvasively assess relative differences in basal neurotransmitter occupancy across regions or ultimately across subject groups.

Study Limitations. There are a number of limitations with this animal model. Studies were performed in isoflurane-anesthetized NHPs to facilitate the use of pharmacological challenges that achieved very high occupancies. Hence, changes in basal DA induced by anesthesia could potentially affect the magnitude of fMRI signal changes in this paradigm. Very high levels of isoflurane (3%) increase basal DA in rats, but effects are not significant at 1% isoflurane (33), as used in this study. In some experiments, we observed large, transient, and repetitive changes in fMRI signal that were consistent with isoflurane-induced burst suppression, a noise source that would not be present in human studies. Additionally, we employed an MRI contrast agent that increases the magnitude of fMRI signal changes. With endogenous contrast techniques, it may be difficult to detect small signal changes due to pharmacological stimuli. The MR contrast agent now has been used for fMRI in human subjects (34), although repeated within-subject measurements presumably would be restricted.

There are also limitations to our interpretation of D2/D3R-mediated neurovascular coupling. Our results and proposed model are consistent with a neurovascular coupling mechanism that is driven by occupancy as one aspect of synaptic processes. However, we cannot exclude direct actions of DA on the vasculature that are uncoupled with neural activity. Our model excludes other factors (e.g., neurotransmitter release) that also

could contribute to neural activity and changes in fMRI signal. Moreover, neural pathways that project to a region of interest may produce functional contributions that are not directly related to local occupancy, although such situations can provide useful information about neural connectivity.

Within the framework of an occupancy-based model like Eq. **1**, there are potential contributions to the fMRI response other than changes in D2/D3R occupancy. We assumed a linear relationship between DA occupancy and fMRI signal, together with a supralinear relationship between RAC and DA occupancies. Although this model produces good agreement with data, there is no routine way to measure DA occupancy directly to verify the linear assumption of Eq. **1**. Additionally, RAC-mediated DA release can cause a positive fMRI signal contribution due to stimulation of D1-like excitatory receptors. To address this issue quantitatively, further studies will be needed to clarify the magnitude of fMRI signal changes associated with changes in D1 occupancy.

Potential Clinical Applications. Clinically, simultaneous PET/fMRI appears to have broad roles for diagnosis and monitoring of therapy (35). On the basis of this study, one potential application is the estimation of basal receptor occupancies, which are coupled to basal neurotransmitter levels. Basal occupancies are not routinely measurable by PET alone unless neurotransmitter is fully depleted from the brain. DA depletion studies have employed PET to assess differences in basal D2/D3R occupancy in patient and control populations (36). Although such studies have helped clarify important aspects of basal DA function, depletion can produce motor dysfunction and "a whole spectrum of psychiatric symptoms" (ref. 37, p. 1755). Other methodological concerns include incomplete depletion and receptor externalization or up-regulation (38). More tolerable methods for assessing basal occupancy might facilitate the identification of therapeutic correlates of basal occupancy, following paths established for D2/D3R occupancy by antipsychotics (39).

In this PET/fMRI study, the DA-bound receptor population was unmasked transiently by antagonist displacement rather than by depletion. If studies demonstrate sufficient reproducibility/specificity, a single injection of an antagonist could in principle provide a relative index of basal occupancy for use in cross-sectional studies. D2/D3R antagonist doses would need to produce measurable fMRI signals in humans while avoiding the noxious side effects that accompany occupancies above the "therapeutic window" of 70–80% for antipsychotics (40).

Conclusions

We demonstrated an imaging methodology in which a PET antagonist can be administered at pharmacologic doses to measure neurovascular responses simultaneously with receptor occupancy. By measuring cerebral responses using different specific activities of [^{11}C]raclopride with PET/fMRI, we observed that the signals from both modalities correlated in anatomical and temporal domains. Our results suggest a monotonic coupling relationship between neurovascular responses and dopamine D2/D3R occupancy in basal ganglia across a wide dynamic range. We observed distinct relative CBV magnitudes between putamen and caudate, consistent with higher basal dopamine levels in putamen. These results demonstrate that the concurrent assessment of hemodynamics and receptor-specific neurotransmission with simultaneous PET/fMRI offers unique possibilities for performing dynamic neurotransmitter mapping and understanding distributed functions of the brain in preclinical and clinical studies.

Materials and Methods

Animal Studies. Two male rhesus macaques, M1 (7 y) and M2 (5 y) with mean weight of 11.7 kg and 7.5 kg underwent imaging. Anesthesia was induced with ketamine (20 mg/kg ketamine with 0.4 mg/kg diazepam or 10 mg/kg ketamine with 0.5 mg/kg xylazene), and a catheter for injections was placed in the saphenous vein. During scans, anesthesia was maintained by isoflurane (0.8–1.5%, mixed with pure oxygen) through an intubation tube without ventilation. Physiological changes (blood pressure, pulse, end-tidal CO_2, and breathing rate) were monitored continuously throughout the experiment. The procedures complied with the regulations of the Subcommittee on Research Animal Care at Massachusetts General Hospital.

Study Design. Four different RAC mass doses were administered by bolus injection to two animals (Table 1). Injections of high-mass doses of RAC were separated by at least 2 wk. Additionally, five low-mass dose studies (three with M1 and two with M2) were acquired to compute average low-dose fMRI signals. An additional mass dose of RAC (1.4 μg/kg) was administered to M1 during a PET-only scan and used in the K_D computation for M1. For each scan, 4.6–6.6 mCi of [^{11}C]RAC was administered intravenously over ~30 s. [^{11}C]RAC was synthesized from the *O*-desmethyl RAC precursor and [^{11}C] methyl iodide. The synthesis and subsequent purification by high-performance liquid chromatography were performed according to ref. 41 with minor modifications. To vary the specific activity and total mass for the five studies, unlabeled RAC was added after synthesis to the saline formulation to obtain the specific activities in Table 1.

PET/fMRI Image Acquisition. Simultaneous dynamic PET/fMRI scans were acquired on a research-dedicated human PET/MR scanner, which consists of a 3 T MRI scanner (MAGNETOM Trio, Tim system; Siemens AG, Healthcare Sector) and an MR-compatible PET insert (BrainPET; Siemens AG, Healthcare Sector). A vendor-supplied circularly polarized local transmit birdcage coil with an eight-channel receive array was used for MR imaging in animal M1. A smaller, more sensitive custom-built eight-channel NHP receive array was used for imaging animal M2. The phased-array receivers enabled a twofold acceleration with GRAPPA (42) in the anterior–posterior direction to reduce the echo time (TE) (TE = 23 ms) and image distortions during fMRI. We employed multislice echo-planar imaging with whole-brain coverage and an isotropic resolution of 1.3 mm (MR field of view = 110 × 72.8 mm^2, bandwidth = 1,350 Hz/pixel) with a temporal resolution (TR) of 3 s. Prior to fMRI, ferumoxytol (Feraheme; AMAG Pharmaceuticals) (43) was administered intravenously at 10 mg/kg to improve fMRI detection power (44). Dynamic acquisition of fMRI images started ~20 min before RAC injection and lasted ~90 min in total.

PET emission data were acquired in list-mode format for 90 min starting with ligand injection and sorted in the line-of-response space. Images were reconstructed with the ordinary Poisson expectation maximization algorithm with 32 iterations. With the PET camera used in this study, the highest image resolution was on the order of 2–3 mm (45). Corrections for scatter and attenuation of the head and the radiofrequency coil were applied during reconstruction as described in ref. 46. The final reconstructed volume consisted of 76 slices with 128 × 128 pixels (2.5-mm isotropic voxels), with framing intervals of 10 × 30 s, followed by 85 × 1 min.

fMRI Data Analysis. fMRI (and PET) data were registered to the Saleem–Logothetis stereotaxic space (47), using a population-averaged MRI-based template for rhesus monkey brain (48). Prior to statistical analysis using the GLM, fMRI data were spatially smoothed with a 2.5-mm Gaussian kernel to correspond approximately to the PET resolution. A gamma-variate function modeled the fMRI temporal response to RAC infusion. The time-to-peak response of the gamma function was adjusted to minimize the χ^2/DOF of the GLM fit to data for mass doses 2–4 (Table 1). The specific binding signal from PET defined the time to peak for the lowest-mass dose, which did not produce observable changes in fMRI signal. Maximum changes in fMRI signal were defined as peak magnitudes of the gamma-variate regressor scaled by the GLM. These values were converted to changes in %CBV, using standard methods (49).

PET Data Analysis. By convention, BP_{ND} is defined at steady-state concentration (50) under the assumption that specific binding has no time dependence. However, binding is not constant in time in this (Fig. 1) or other challenge protocols, so that it is unclear how BP_{ND} relates to dynamic fMRI measures. Nevertheless, we report BP_{ND} values, using a conventional analysis to facilitate literature comparisons. Additionally, we employed an alternative analysis that explicitly incorporates time dependence into occupancy estimates and allows the comparison of peak occupancy with peak CBV measures. We thus defined a related binding-dependent quantity, the dynamic binding potential, $DBP_{ND}(t)$:

$$DBP_{ND}(t) \equiv \frac{R_1 \cdot k_2'}{k_{2a}(t)} - 1. \quad [3]$$

$DBP_{ND}(t)$ was determined using a time-dependent parameter $k_{2a}(t) = k_{2a} + k_{2a\gamma}(t/\tau \cdot e^{(1-t/\tau)})$ from the SRTM (51, 52). This enabled computation of peak occupancies:

$$\hat{\theta}_{RAC}^{peak} \equiv \max\left(\frac{\Delta DBP_{ND}(t)}{DBP_{ND}^{(0)}}\right) \approx \theta_{RAC}^{peak}. \quad [4]$$

The term DBP_{ND}^{peak} (e.g., Table 1) is the DBP_{ND} value that corresponds to the peak occupancy as defined in Eq. **4**.

PET data were analyzed using the cerebellum ROI as a reference region, where D2/D3R concentration has been reported to be 10^3 times smaller than in putamen (53). Although nonnegligible specific binding to D2/D3R may be detectable with other ultrahigh-affinity ligands, [^{11}C]RAC has negligible specific binding in the cerebellum (54). BP_{ND} values were obtained with the multilinear reference tissue model (MRTM) (55), using the standard three independent parameters R_1, k_{2a}, and k'_2. Alternatively, we employed the two-parameter MRTM2 (55) and included the time-varying parameter $k_{2a}(t)$, following existing methods (51, 52). This dynamic analysis was applied to determine peak RAC occupancy $\hat{\theta}_{RAC}^{peak}$ from Eq. **4**, using the maximum value of the $k_{2a}(t)$ curve. Simulations demonstrated that MRTM2 with a time-dependent $k_{2a}(t)$ provides a more accurate determination of peak occupancy than the conventional three-parameter implementation of SRTM for large doses of RAC (Fig. S3). Specific binding estimates were derived by subtracting cerebellum TACs from other ROIs after inclusion of the R_1 term from SRTM: $\hat{S} = C_T - R_1 C_{REF}$. Parametric images were generated using voxel-wise modeling based upon publicly available software (www.nitrc.org/projects/jip).

ACKNOWLEDGMENTS. We thank Helen Deng, Steve Carlin, Chris Moseley, Grae Arabasz, and Shirley Hsu for their help with animal preparation and monitoring, [^{11}C]RAC synthesis, and PET/MR scanning. National Institutes of Health Grants R90DA023427, P41RR14075, P30DA28800, S10RR026666, S10RR017208, S10RR022976, and S10RR019933 supported this research.

1. Fox PT, Raichle ME, Mintun MA, Dence C (1988) Nonoxidative glucose consumption during focal physiologic neural activity. *Science* 241(4864):462–464.
2. Davis TL, Kwong KK, Weisskoff RM, Rosen BR (1998) Calibrated functional MRI: Mapping the dynamics of oxidative metabolism. *Proc Natl Acad Sci USA* 95(4):1834–1839.
3. Hoge RD, et al. (1999) Linear coupling between cerebral blood flow and oxygen consumption in activated human cortex. *Proc Natl Acad Sci USA* 96(16):9403–9408.
4. Roy CS, Sherrington CS (1890) On the regulation of the blood-supply of the brain. *J Physiol* 11(1–2):85–158.17.
5. Logothetis NK, Pauls J, Augath M, Trinath T, Oeltermann A (2001) Neurophysiological investigation of the basis of the fMRI signal. *Nature* 412(6843):150–157.
6. Devor A, et al. (2003) Coupling of total hemoglobin concentration, oxygenation, and neural activity in rat somatosensory cortex. *Neuron* 39(2):353–359.
7. Sheth SA, et al. (2004) Linear and nonlinear relationships between neuronal activity, oxygen metabolism, and hemodynamic responses. *Neuron* 42(2):347–355.
8. Judenhofer MS, et al. (2008) Simultaneous PET-MRI: A new approach for functional and morphological imaging. *Nat Med* 14(4):459–465.
9. Elsinga PH, Hatano K, Ishiwata K (2006) PET tracers for imaging of the dopaminergic system. *Curr Med Chem* 13(18):2139–2153.
10. Chen YI, et al. (1999) Detection of dopaminergic cell loss and neural transplantation using pharmacological MRI, PET and behavioral assessment. *Neuroreport* 10(14):2881–2886.
11. Chen Y-C, Choi J-K, Andersen SL, Rosen BR, Jenkins BG (2005) Mapping dopamine D2/D3 receptor function using pharmacological magnetic resonance imaging. *Psychopharmacology* 180(4):705–715.
12. Choi J-K, Chen YI, Hamel E, Jenkins BG (2006) Brain hemodynamic changes mediated by dopamine receptors: Role of the cerebral microvasculature in dopamine-mediated neurovascular coupling. *Neuroimage* 30(3):700–712.
13. Traynor JR, Neubig RR (2005) Regulators of G protein signaling & drugs of abuse. *Mol Interv* 5(1):30–41.
14. Rabiner EA, et al. (2009) In vivo quantification of regional dopamine-D3 receptor binding potential of (+)-PHNO: Studies in non-human primates and transgenic mice. *Synapse* 63(9):782–793.
15. Lammertsma AA, Hume SP (1996) Simplified reference tissue model for PET receptor studies. *Neuroimage* 4(3 Pt 1):153–158.
16. Worsley KJ, et al. (2002) A general statistical analysis for fMRI data. *Neuroimage* 15(1):1–15.
17. Carson RE, et al. (1997) Quantification of amphetamine-induced changes in [11C]raclopride binding with continuous infusion. *J Cereb Blood Flow Metab* 17(4):437–447.
18. Narendran R, et al. (2005) Measurement of the proportion of D2 receptors configured in state of high affinity for agonists in vivo: A positron emission tomography study using [11C]N-propyl-norapomorphine and [11C]raclopride in baboons. *J Pharmacol Exp Ther* 315(1):80–90.
19. Mandeville JB, et al. (2013) A receptor-based model for dopamine-induced fMRI signal. *Neuroimage* 75C:46–57.
20. Urban NBL, et al. (2012) Imaging human reward processing with positron emission tomography and functional magnetic resonance imaging. *Psychopharmacology* 221(1): 67–77.
21. Schott BH, et al. (2008) Mesolimbic functional magnetic resonance imaging activations during reward anticipation correlate with reward-related ventral striatal dopamine release. *J Neurosci* 28(52):14311–14319.
22. Laruelle M (2000) Imaging synaptic neurotransmission with in vivo binding competition techniques: A critical review. *J Cereb Blood Flow Metab* 20(3):423–451.
23. Clark AJ (1970) *General Pharmacology* (Springer, Berlin), pp 61–98, 176–206, and 215–217.
24. Ekstrom A (2010) How and when the fMRI BOLD signal relates to underlying neural activity: The danger in dissociation. *Brain Res Brain Res Rev* 62(2):233–244.
25. Hertel P, Fagerquist MV, Svensson TH (1999) Enhanced cortical dopamine output and antipsychotic-like effects of raclopride by alpha2 adrenoceptor blockade. *Science* 286(5437):105–107.
26. Skirboll S, Wang J, Mefford I, Hsiao J, Bankiewicz KS (1990) In vivo changes of catecholamines in hemiparkinsonian monkeys measured by microdialysis. *Exp Neurol* 110(2):187–193.
27. Pifl C, Hornykiewicz O (2006) Dopamine turnover is upregulated in the caudate/putamen of asymptomatic MPTP-treated rhesus monkeys. *Neurochem Int* 49(5):519–524.
28. Goldstein DS, et al. (2011) Catechols in post-mortem brain of patients with Parkinson disease. *Eur J Neurol* 18(5):703–710.
29. Riccardi P, et al. (2008) Estimation of baseline dopamine D2 receptor occupancy in striatum and extrastriatal regions in humans with positron emission tomography with [18F] fallypride. *Biol Psychiatry* 63(2):241–244.
30. Kegeles LS, et al. (2010) Increased synaptic dopamine function in associative regions of the striatum in schizophrenia. *Arch Gen Psychiatry* 67(3):231–239.
31. Martinez D, et al. (2009) Lower level of endogenous dopamine in patients with cocaine dependence: Findings from PET imaging of D(2)/D(3) receptors following acute dopamine depletion. *Am J Psychiatry* 166(10):1170–1177.
32. Morissette M, Di Paolo T (2009) Effect of estradiol on striatal dopamine activity of female hemiparkinsonian monkeys. *J Neurosci Res* 87(7):1634–1644.
33. Adachi YU, et al. (2005) Isoflurane anesthesia induces biphasic effect on dopamine release in the rat striatum. *Brain Res Bull* 67(3):176–181.
34. Qiu D, Zaharchuk G, Christen T, Ni WW, Moseley ME (2012) Contrast-enhanced functional blood volume imaging (CE-fBVI): Enhanced sensitivity for brain activation in humans using the ultrasmall superparamagnetic iron oxide agent ferumoxytol. *Neuroimage* 62(3):1726–1731.
35. Catana C, Drzezga A, Heiss W-D, Rosen BR (2012) PET/MRI for neurologic applications. *J Nucl Med* 53(12):1916–1925.
36. Booij L, Van der Does AJ, Riedel WJ (2003) Monoamine depletion in psychiatric and healthy populations: Review. *Mol Psychiatry* 8(12):951–973.
37. de Haan L, Booij J, Lavalye J, van Amelsvoort T, Linszen D (2005) Subjective experiences during dopamine depletion. *Am J Psychiatry* 162(9):1755.
38. Guo N, et al. (2003) Dopamine depletion and in vivo binding of PET D1 receptor radioligands: Implications for imaging studies in schizophrenia. *Neuropsychopharmacology* 28(9):1703–1711.
39. Uchida H, et al. (2011) Dopamine D2 receptor occupancy and clinical effects: A systematic review and pooled analysis. *J Clin Psychopharmacol* 31(4):497–502.
40. Nord M, Farde L (2011) Antipsychotic occupancy of dopamine receptors in schizophrenia. *CNS Neurosci Ther* 17(2):97–103.
41. Farde L, et al. (1985) Substituted benzamides as ligands for visualization of dopamine receptor binding in the human brain by positron emission tomography. *Proc Natl Acad Sci USA* 82(11):3863–3867.
42. Griswold MA, et al. (2002) Generalized autocalibrating partially parallel acquisitions (GRAPPA). *Magn Reson Med* 47(6):1202–1210.
43. Bernd H, De Kerviler E, Gaillard S, Bonnemain B (2009) Safety and tolerability of ultrasmall superparamagnetic iron oxide contrast agent: Comprehensive analysis of a clinical development program. *Invest Radiol* 44(6):336–342.
44. Mandeville JB (2012) IRON fMRI measurements of CBV and implications for BOLD signal. *Neuroimage* 62(2):1000–1008.
45. Kolb A, et al. (2012) Technical performance evaluation of a human brain PET/MRI system. *Eur Radiol* 22(8):1776–1788.
46. Catana C, et al. (2010) Toward implementing an MRI-based PET attenuation-correction method for neurologic studies on the MR-PET brain prototype. *J Nucl Med* 51(9):1431–1438.
47. Saleem KS, Logothetis NK (2006) *A Combined MRI and Histology Atlas of the Rhesus Monkey Brain* (Elsevier, Burlington, MA). Available at http://public.eblib.com/EBLPublic/PublicView.do?ptiID=283976.
48. McLaren DG, et al. (2009) A population-average MRI-based atlas collection of the rhesus macaque. *Neuroimage* 45(1):52–59.
49. Mandeville JB, et al. (1998) Dynamic functional imaging of relative cerebral blood volume during rat forepaw stimulation. *Magn Reson Med* 39(4):615–624.
50. Innis RB, et al. (2007) Consensus nomenclature for in vivo imaging of reversibly binding radioligands. *J Cereb Blood Flow Metab* 27(9):1533–1539.
51. Normandin MD, Schiffer WK, Morris ED (2012) A linear model for estimation of neurotransmitter response profiles from dynamic PET data. *Neuroimage* 59(3):2689–2699.
52. Alpert NM, Badgaiyan RD, Livni E, Fischman AJ (2003) A novel method for noninvasive detection of neuromodulatory changes in specific neurotransmitter systems. *Neuroimage* 19(3):1049–1060.
53. Hall H, et al. (1996) Autoradiographic localization of extrastriatal D2-dopamine receptors in the human brain using [125I]epidepride. *Synapse* 23(2):115–123.
54. Pinborg LH, et al. (2007) [123I]epidepride binding to cerebellar dopamine D2/D3 receptors is displaceable: Implications for the use of cerebellum as a reference region. *Neuroimage* 34(4):1450–1453.
55. Ichise M, et al. (2003) Linearized reference tissue parametric imaging methods: Application to [^{11}C]DASB positron emission tomography studies of the serotonin transporter in human brain. *J Cereb Blood Flow Metab* 23(9):1096–1112.